






Research Article

Trinary Component Adsorption of Methylene Blue, Methyl Orange, and Methyl Red from Aqueous Solution Using TiO₂/Activated Carbon

Nguyen Thi Thanh Tu ¹, Tran Si Thanh,^{2,3} Phan Tu Quy ⁴, Tran Thi Minh Ha,⁴ Phan Thi Kim Thu,⁴ Nguyen Hong Bich,² Le Van Thanh Son,⁵ Vo Thang Nguyen,⁵ Dao Ngoc Nhiem ⁶, Pham Khac Lieu ⁷, and Dinh Quang Khieu ²

¹Faculty of Applied Technology, School of Engineering and Technology, Van Lang University, 700000, Vietnam

²University of Sciences, Hue University, 530000, Vietnam

³Dak Nong Department of Education and Training, 640000, Vietnam

⁴Tay Nguyen University, 630000, Vietnam

⁵University of Education and Science, The University of Danang, 500000, Vietnam

⁶Institute of Materials Sciences, VAST, 100000, Vietnam

⁷Hue University, 530000, Vietnam

Correspondence should be addressed to Nguyen Thi Thanh Tu; tu.ntt@vlu.edu.vn and Dinh Quang Khieu; dqkhieu@hueuni.edu.vn

Received 18 May 2022; Revised 26 August 2022; Accepted 13 October 2022; Published 20 January 2023

Academic Editor: Anjani Ravi Kiran Gollakota

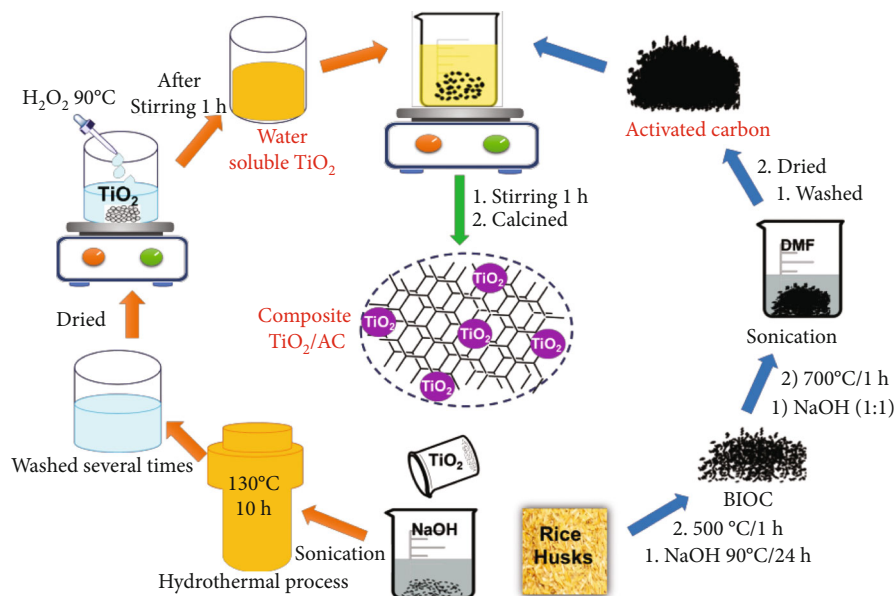
Copyright © 2023 Nguyen Thi Thanh Tu et al. This is an open access article distributed under the Creative Commons Attribution License, which permits unrestricted use, distribution, and reproduction in any medium, provided the original work is properly cited.

Porous TiO₂/activated carbon (AC) material was synthesized by grafting peroxy-hydro titanium complexes to rice husk-derived activated carbon. It was found that the morphology of TiO₂/AC consists of TiO₂ fine particles highly dispersed on the AC matrix. The obtained TiO₂/AC composites with high surface area and a red shift exhibit an excellent adsorption performance in both single and trinary system toward methylene blue (MB), methyl orange (MO), and methyl red (MR). The isotherm models including extended Langmuir, P-factor, ideal adsorbed solution theory (IAST) for Langmuir, Freundlich, and Sips models were applied to study the adsorption equilibrium data of trinary solutions. It was found that IAST for Freundlich and Langmuir models were the most suitable one to describe the adsorption of the three dyes on TiO₂/AC material. The high maximum adsorption capacities (mmol g⁻¹) in single/trinary mixture were found as 0.452/0.340 for MB; 0.329/0.321 for MO; and 0.806/2.04 for MR. Moreover, the recyclability experiments showed that the adsorbent could be reused through photocatalytic self-cleaning for at least three cycles with stable capacity. Thus, the TiO₂/AC can be effectively employed for the removal of dyes from industrial textile wastewater.

1. Introduction

Dye pollutants in wastewater are a critical environmental issue due to their nonbiodegradable and toxic nature which can generate serious threats to human being and marine organism. The dyeing wastewater discharged from industrial textiles is highly visible and undesirable even at low concentrations of dyes. Hence, the dyes must be effectively eliminated from the dyestuff wastewater to clear up the

biological, ecological, and industrial issues. Therefore, various physical-chemistry treatment methods, including chemical ion exchange [1], membrane filtration [2], physical adsorption [3], photocatalytic [4], and biological approaches [5], have been developed to remove dyestuff from effluents. Among these, the adsorption approach has been considered as a promising method for treatment of discharged wastewater due to its easy operation, high efficiency, and economic feasibility. The nature of the adsorbent is one of the



SCHEME 1: The diagram of synthesis of TiO_2/AC from soluble-water titanium and rice husk-derived activated carbon.

important factors deciding the effectiveness of any adsorption processes. The adsorbents with low cost, high adsorption capacity, and easy recyclability are desirable in the adsorption removal of dye molecules. The use of activated carbon prepared from rich-carbon biomasses for removing pollutants from wastewater has been intensively investigated because of its high synthesis yield, cheapness, eco-friendliness, and great adsorption efficiency [6]. However, the recycling of activated carbon material for further use usually involves organic solvents, resulting in secondary pollutants. A more eco-friendly strategy to recycle these adsorbents is photocatalytic self-cleaning activities through grafting other catalytically reactive species such as metal halides, metal oxides, and metal sulfides on various carbon matrixes. TiO_2 nanoparticles is a well-known photocatalyst in advanced oxidation process which can mineralize organic pollutants under UV irradiation. However, there are some disadvantages of using TiO_2 in powder form during the photocatalytic process: (i) titanium sources such as titanium alkoxides and titanium chlorides are difficult to handle due to its instability in moisture atmospheres; (ii) the fine powder TiO_2 is likely to aggregate to form larger particles. These issues can be solved by using soluble-water titanium complexes instead of traditional easily hydrolyzed titanium sources. Therefore, the construction of heterojunctions by hybridizing activated carbon with water-soluble titanium complexes derived catalytically reactive TiO_2 is an effective method to improve for recycling through photocatalytic self-cleaning.

Although there is a great availability of research information on single-component adsorption [7–10] or binary-component adsorption [11, 12], that for complex mixture is more limited which leaves the adsorption of most industries discharge wastewater containing several components unexplainable. Gurav et al. presented the adsorption of the binary mixture containing bisphenol-A and solvent black-3 dye mix-

tures onto biochar by using Langmuir isotherm model [13]. Adsorption of safranin O and methylene blue dyes from single and binary systems using Langmuir, Freundlich, Temkin, and Dubinin–Radushkevich model was also reported [14]. According to our best knowledge, the study on adsorption isotherms of trinary component system is less available.

In this study, we synthesized a three-dimensional $\text{TiO}_2/\text{activated carbon}$ (TiO_2/AC) via peroxy-hydroxy titanium (IV) complexes and activated carbon derived from rice husks for eliminating the pollutants from aqueous solution. Three organic compounds including methylene blue (MB), methyl orange (MO), and methyl red (MR) were used as model pollutants to investigate their adsorption on $\text{TiO}_2/\text{activated carbon}$ (TiO_2/AC) in single/trinary component systems using extended Langmuir, P-factor model, ideal adsorbed solution theory for Langmuir, Freundlich, and Sips models. The main objective of this work is to investigate the simultaneous removal of both anionic and cationic dyes from the single/trinary systems. Furthermore, the recyclability of the TiO_2/AC was performed by the photocatalytic self-cleaning.

2. Experimental Methods

2.1. Materials. Rice husks were collected from local area (Hue city, Vietnam). All chemicals were used as received without any further purification. Anatase (TiO_2 ; Merck, Germany, 99%), sodium (NaOH ; Guangzhou, China, 97%), acid chlorhydride (HCl ; Guangzhou, China, 36%), hydroperoxide (H_2O_2 30% Guangzhou, China), methylene blue (MB, $\text{C}_{16}\text{H}_{18}\text{ClN}_3\text{S}$), methyl orange (MO, $\text{C}_{14}\text{H}_{14}\text{N}_3\text{NaO}_3\text{S}$), methyl red (MR, $\text{C}_{15}\text{H}_{15}\text{N}_3\text{O}$), and N,N-Dimethylformamide (DMF) were used in this work.

2.2. Synthesis of the Peroxy-Hydroxy Titanium Complexes and Activated Carbon. TiO_2 was synthesized by ultrasonically assisted hydrothermal method. 0.25 grams of TiO_2

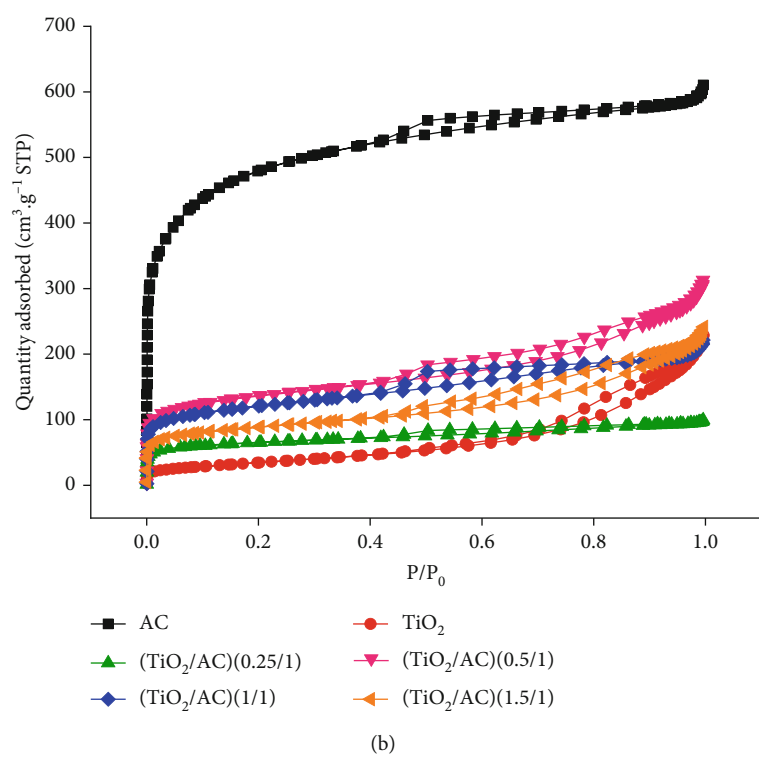
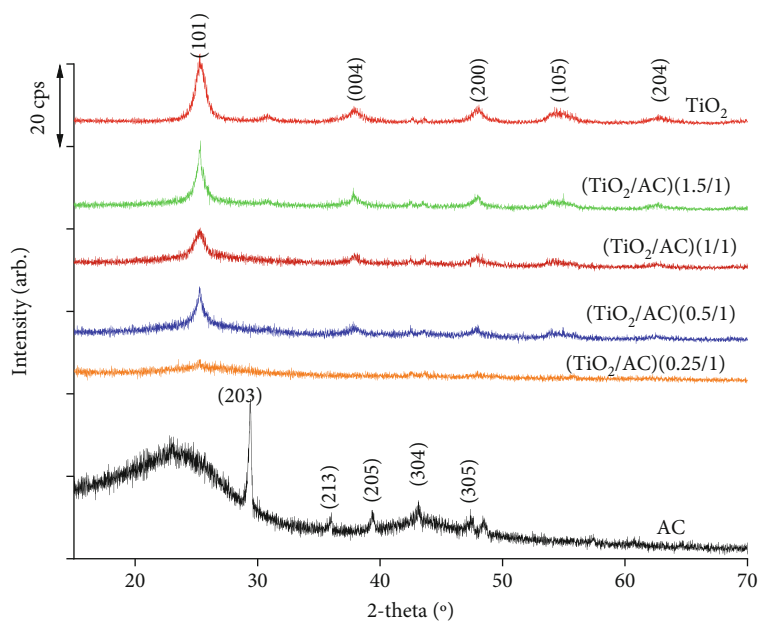


FIGURE 1: Continued.

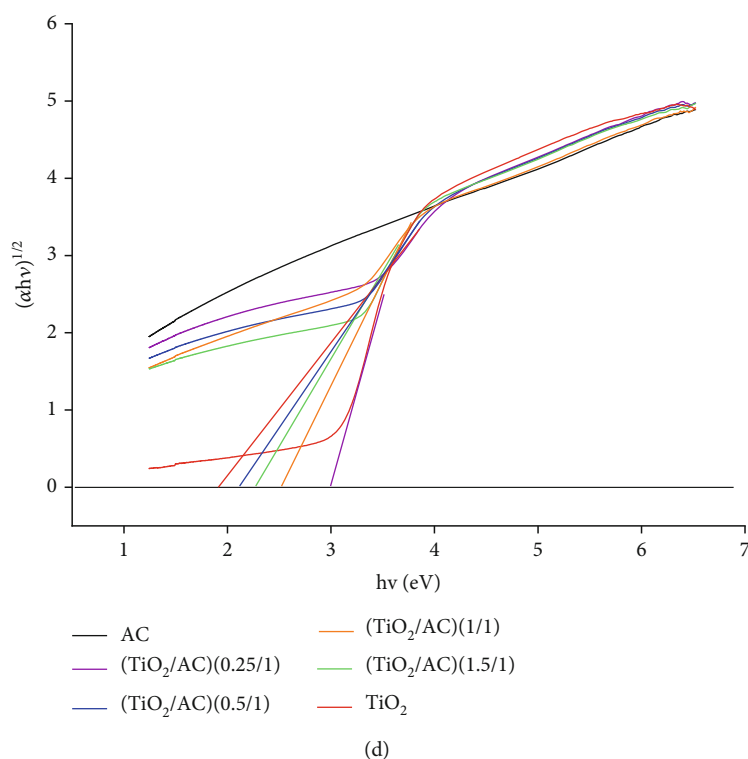
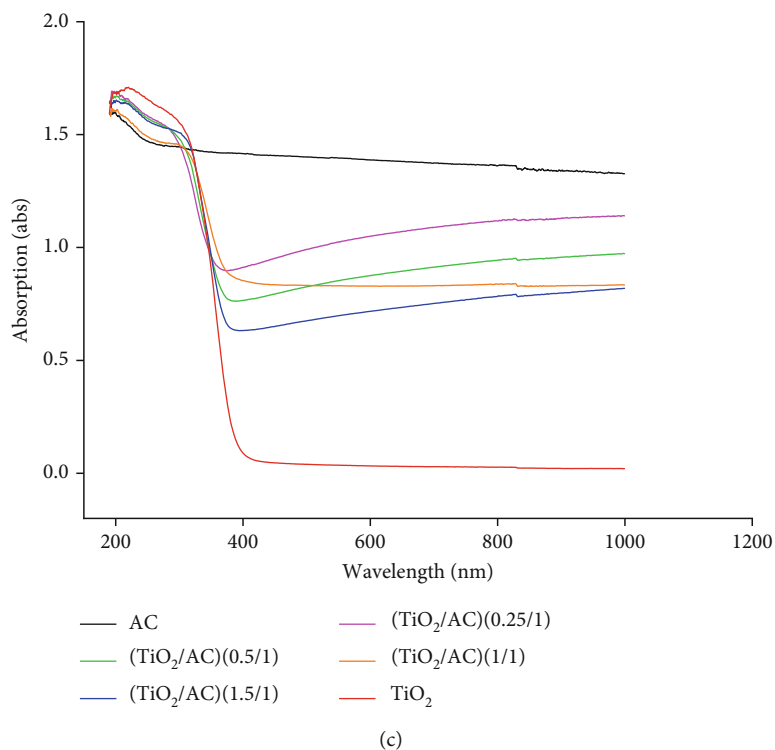


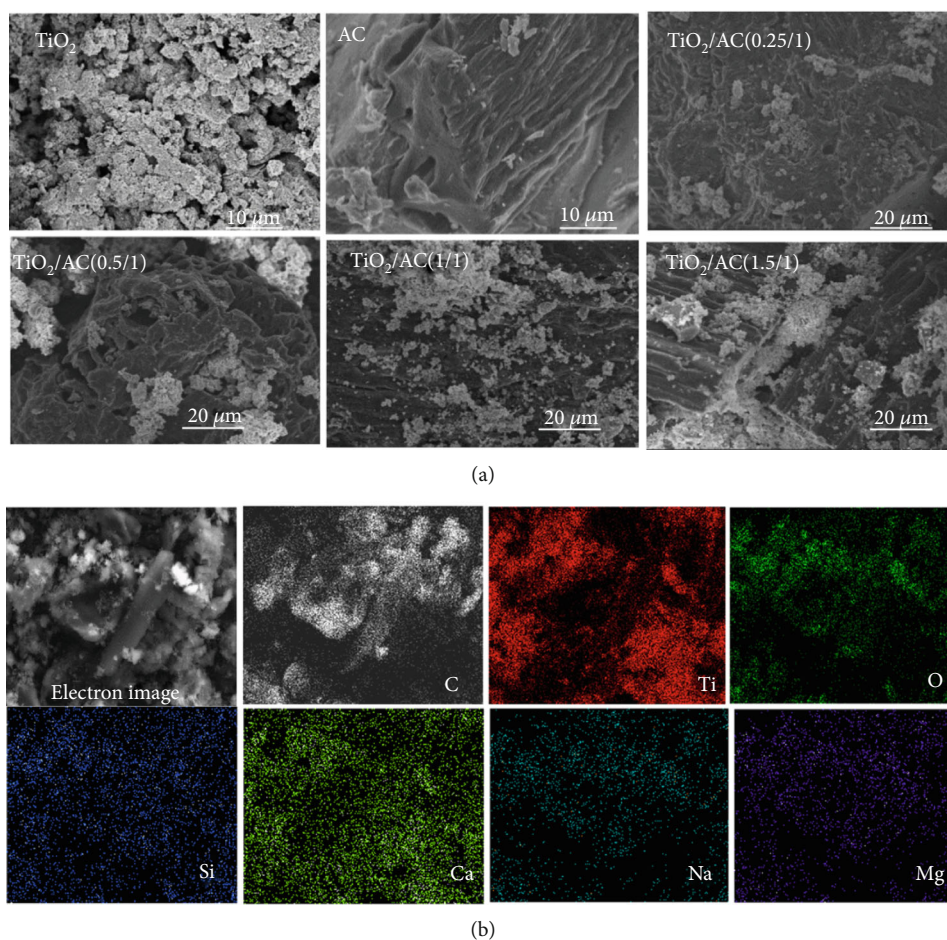
FIGURE 1: (a) XRD patterns, (b) nitrogen adsorption/desorption isotherms, (c) UV-Vis diffuse reflectance spectroscopy, and (d) Tauc's plots of AC, TiO₂/AC (0.25/1), TiO₂/AC (0.5/1), TiO₂/AC (1/1), TiO₂/AC (1.5/1), and TiO₂.

powder was dispersed into a teflon flask containing 12.5 mL of 20 M NaOH solution before being processed by ultrasonic for 30 minutes. The teflon bottle was then inserted in the autoclave and kept at 130°C for 10 h. After the hydrothermal process, the autoclave was naturally cooled to room temper-

ature. The mixture was then washed several times with 0.1 M HCl and distilled water until the pH of supernatant was neutral. The product was dried in vacuum at 100°C for 6 h. 0.25 grams obtained product was mixed with 35 mL of H₂O₂ at 90°C with magnetic stirring for an hour to form a yellow

TABLE 1: Textural properties of AC, TiO₂, and TiO₂/AC composites.

Materials	Surface area based on BET model (m ² g ⁻¹)	Porous volume (cm ³ /g)	Mesoarea (m ² g ⁻¹)	Microarea (m ² g ⁻¹)
AC	1713	610	333	1380
TiO ₂	124	228	94	31
TiO ₂ /AC (0.25/1)	238	100	108	131
TiO ₂ /AC (0.5/1)	494	313	206	288
TiO ₂ /AC (1/1)	436	222	193	243
TiO ₂ /AC (1.5/1)	320	241	182	138

FIGURE 2: (a) SEM observation of TiO₂/AC composites and (b) EDX mapping of TiO₂/AC (0.5/1).

transparent peroxy-hydroxy titanium complex solution (0.25 grams TiO₂/35 mL).

The preparation of activated carbon from rice husk consists of two steps: firstly 60 grams of rice husks was soaked in 800 mL of 1 M NaOH and placed in an oven at 90°C for 24 h. The rice husks were then collected, washed, and calcined at 500°C for an hour to obtain the biochar. After that, 2 grams of biochar was mixed with 2 grams of NaOH in a Ni crucible and heated at 700°C for 2 h. The resulting product was washed with distilled water to completely remove all the excess NaOH, followed by ultrasonic treatment in DMF for 1 hour. The solid was separated by the centrifugation and

dried at 100°C for 24 h to obtain the activated carbon (denoted as AC).

The TiO₂/AC composites with different TiO₂/AC mass ratio were prepared through ultrasonic mixing of a specific volume of titanium complex solution (17.5, 35.0, 70.0, and 105.0 mL equivalent to 0.125, 0.250, 0.500, and 0.750 grams of TiO₂, respectively) and 0.5 grams of AC, after sonication for 1 h the mixture is dried at 80°C for 6 hours. The resultant powders were calcined at 350°C for 2 hours in oxygen-free atmosphere. The TiO₂/AC composites was denoted as TiO₂/AC (0.25/1), TiO₂/AC (0.5/1), TiO₂/AC (1/1), and TiO₂/AC (1.5/1) with the numbers in parenthesis presenting

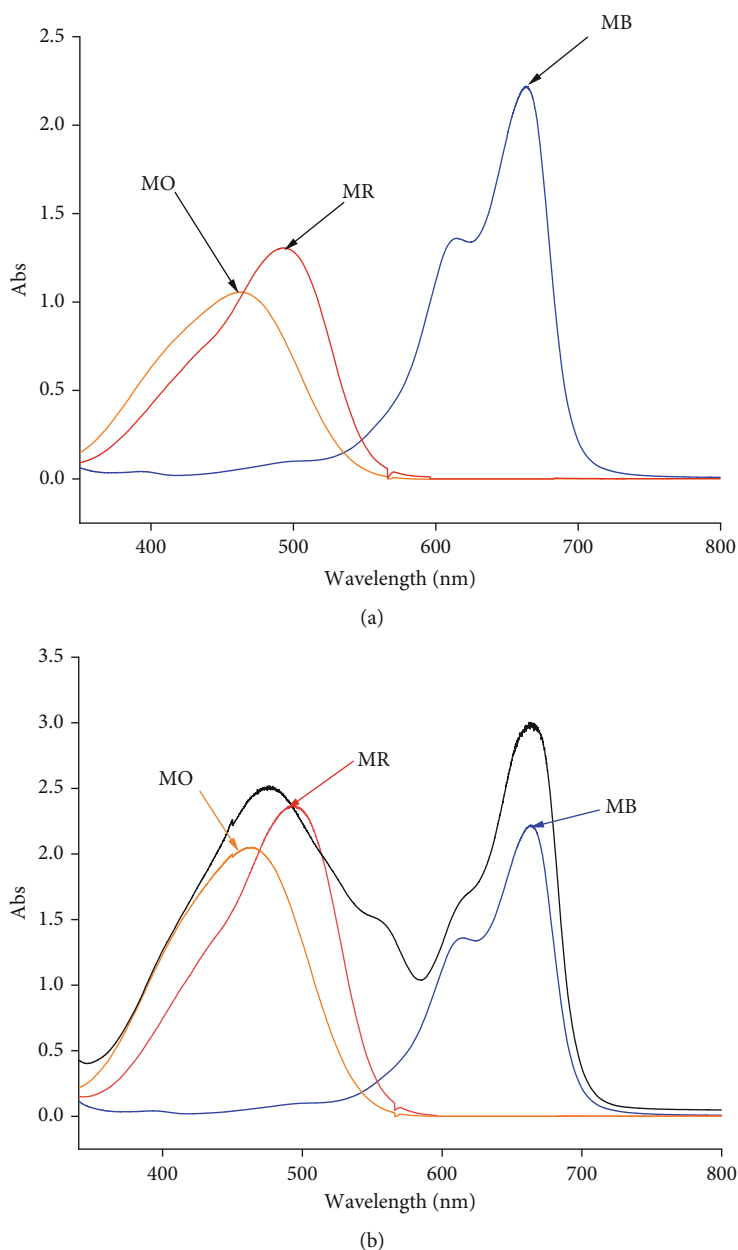


FIGURE 3: (a) The UV-Vis spectra of MB, MO, and MR individual (0.0625 mM MB, 0.061 mM MO, and 0.111 mM MR) and (b) UV-Vis spectrum of trinary mixture of MB, MO, and MR as well as corresponding UV-Vis deconvulated spectra (Trinary component mixture of 0.0625 MB, 0.061 MO, and 0.111 MR, mass of adsorbent).

the ratio of TiO_2/AC in weight. The schematic diagram of TiO_2/AC synthesis is illustrated in the Scheme 1.

2.3. Adsorption Experiments

2.3.1. Adsorption Isotherm in Single Component Solution

(1) *Determination of the Isoelectric Point of TiO_2/AC .* 10 mg TiO_2/AC was dispersed into 100 mL conical flasks containing 25 mL 0.1 M NaCl, and the pH_i of solution was adjusted in the range of 2-12 by adding 0.01 M HCl and 0.01 M NaOH solution. The sample was shaken in the dark for 24 h at a constant speed of 200 rpm and the pH_f of the supernatant was then measured. The pH of point of zero charge

was derived from the plot of $\Delta\text{pH} = \text{pH}_f - \text{pH}_i$ versus pH_i where $\Delta\text{pH} = 0$.

(2) *Single Component Isotherm Studies.* To study isotherm adsorption in the single component system, 0.1, 0.2, 0.3, 0.4, 0.5, 0.6, and 0.7 grams of TiO_2/AC were added into a series of seven flasks containing 200 mL solution of individual dyes at concentration of 0.0469 mM, 0.0458 mM, and 0.0743 mM for MB, MO, and MR, respectively. These flasks were shaken in the dark for 24 hours to ensure adsorption/desorption equilibrium. The dye concentration in the supernatant was measured by UV-Vis spectrophotometry at its corresponding adsorption maxima.

TABLE 2: The parameters of adsorption isotherms of Langmuir, Freundlich, and Temkin models for TiO₂/AC (0.5/1), TiO₂, and AC in single component system of MB, MO, and MR.

Adsorbent	Dyes	Langmuir isotherm model			Freundlich isotherm model			Temkin isotherm model		
		q_m (mmol g ⁻¹)	a_L (L g ⁻¹)	R^2	b_F	K_F (L g ⁻¹)	R^2	K_T (L g ⁻¹)	b_T (KJ.mol ⁻¹)	R^2
AC		0.865	0.139	0.989	1.737	49.854	0.993	589.03	13.39	0.986
TiO ₂ /AC	MB	0.452	0.094	0.997	1.744	18.683	0.998	256.19	23.51	0.997
TiO ₂		0.200	0.084	0.999	1.932	9.072	0.999	205.23	49.17	0.999
AC		0.532	0.539	0.993	4.706	87.207	0.991	4682.30	28.00	0.992
TiO ₂ /AC	MO	0.329	0.390	0.988	2.686	37.545	0.995	1366.62	35.12	0.991
TiO ₂		0	0	—	0	0	—	0	0	—
AC		1.219	0.152	0.979	2.129	64.512	0.951	359.84	8.82	0.982
TiO ₂ /AC	MR	0.806	0.305	0.998	3.116	75.239	0.908	0.80	5.48	0.823
TiO ₂		0	0	—	0	0	—	0	0	—

The adsorption capacity (q_t) at a certain time and (q_e) at the equilibrium time for each dye are expressed as follows:

$$q_t = \frac{(C_i - C_f)V}{m}, \quad (1)$$

$$q_e = \frac{(C_i - C_e)V}{m}, \quad (2)$$

where C_i (mM) and C_e (mM) are the concentration of dyes at a certain and equilibrium time in the solution, respectively; V and m are the solution volume (L) and mass of adsorbent (g).

Three isotherms were used to investigate the adsorption of three dyes onto TiO₂/AC, namely, Langmuir [15], Freundlich [16], Sips [17], and Temkin [18] isotherms as expressed in

$$q_e = \frac{K_L \cdot C_e}{1 + a_{L,i} C_e} \text{ Langmuir isotherm,} \quad (3)$$

$$q_e = a_F \cdot C_e^{b_F} \text{ Freundlich isotherm,} \quad (4)$$

$$q_e = \frac{K_S \cdot C_e^{1/b_S}}{1 + a_S C_e^{1/b_S}} \text{ Sips isotherm,} \quad (5)$$

$$q_e = \frac{RT}{b_T} \ln R_T \cdot C_e \text{ Temkin isotherm,} \quad (6)$$

where q_e and C_e present adsorption capacity (mmol g⁻¹) and concentration (mM) at equilibrium, and K_L (L.g⁻¹) and a_L (L.mM⁻¹), a_F and b_F , K_S , a_S (L.mM⁻¹), and b_S , and A_T (L.g⁻¹), b_T , R (8.314 x 10⁻³ J.mM⁻¹.K⁻¹), T (298 K), and $B = RT/b_T$ are the constants of Langmuir, Freundlich, Sips, and Temkin models, respectively.

2.3.2. Adsorption Study of Multicomponent System

(1) *Effect of pH on the Simultaneous Adsorption of the Mixture of Three Chosen Dyes onto TiO₂/AC Adsorbent.* The influence of pH on dye absorption of TiO₂/AC was studied by determining the dye uptake in a mixture of three dyes at different pH. The experiments were conducted on 200 mL solution containing 0.0469 mM MB, 0.0458 mM

MO, and 0.0743 mM MR with the presence of 10 mg of TiO₂/AC. The pH of solution was adjusted from 2 to 12 by adding 0.01 M HCl and 0.01 M NaOH solution. The samples were kept in the dark and were shaken at a constant speed of 200 rpm for 4 h to achieve adsorption equilibrium conditions. Afterwards, the samples were centrifuged at 4500 rpm for around 15 min to separate the supernatant for UV-Vis measurement at corresponding maximum absorbance wavelength to determine the residual concentrations of each dye.

(2) *Multicomponent Isotherm Studies.* The adsorption equilibrium of multicomponent system was investigated in a similar manner in a 200 mL mixtures of 0.0469 mM MB, 0.0458 mM MO, and 0.0743 mM MR.

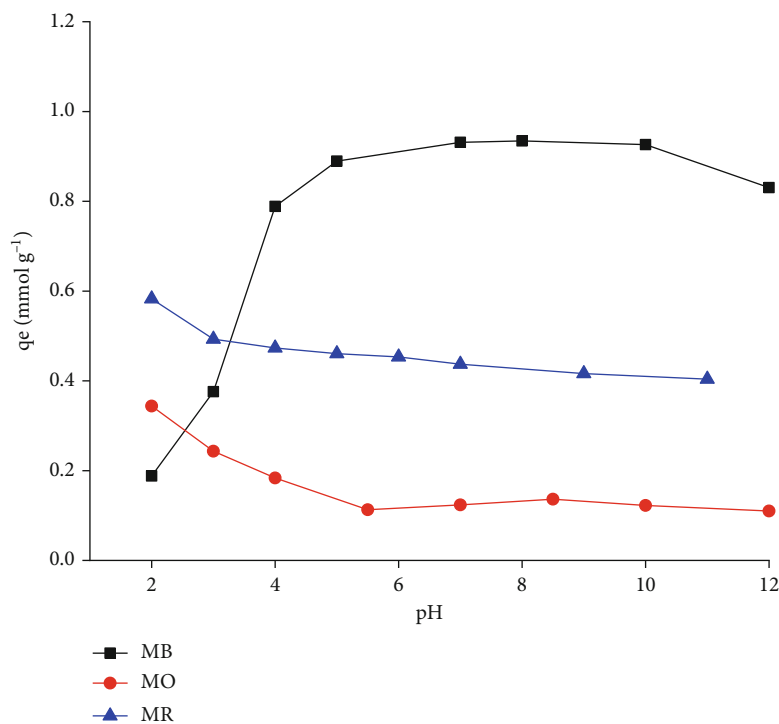
The extended Langmuir, P-factor models, and ideal adsorbed solution theory (IAST) incorporating three different isotherm models of Langmuir, Freundlich, and Sips equations were used to examine the ternary dye system. Theory of these models is presented in detail in references [10, 11].

A model for competitive sorption based on the Langmuir equation (extended Langmuir (EL)) was first proposed by Butler and Ockrent [19] to express the adsorption equilibrium in multicomponent systems. This isotherm is applicable as each component obeys Langmuir behavior in a single-solute system.

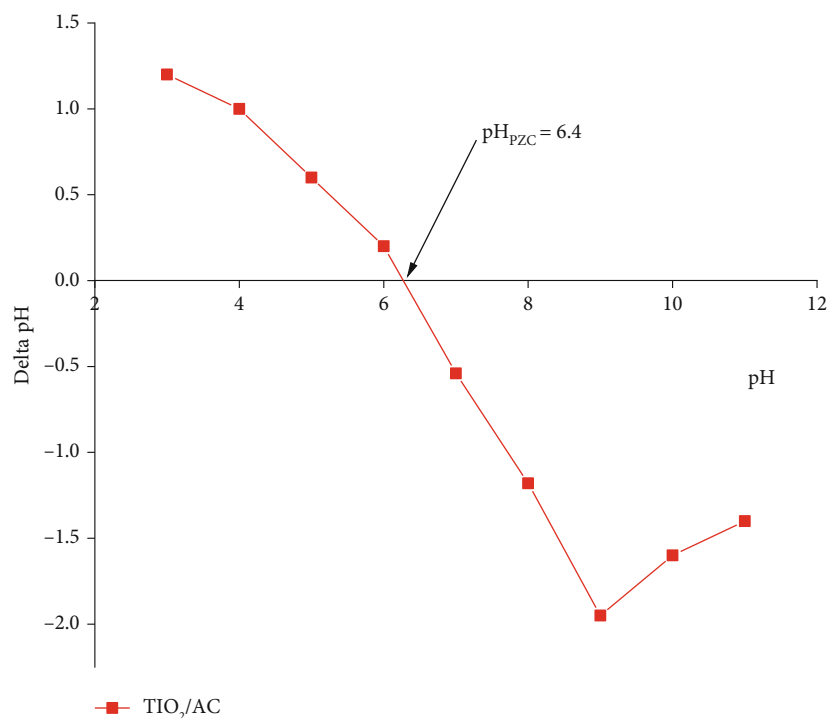
$$q_{e,i} = \frac{K_{L,i} \cdot C_{e,i}}{1 + \sum a_{L,i} C_{e,i}}, \quad (7)$$

where $q_{e,i}$ and $C_{e,i}$ present adsorption capacity (mmol.g⁻¹) and concentration (mM) of component i at equilibrium, and $K_{L,i}$ (L.g⁻¹) and $a_{L,i}$ (L.mM⁻¹) are Langmuir constants of component i .

The P-factor method can be employed to investigate the competitive adsorption behavior of dyes in the ternary component system. This model presumed a simplified approach to correlate and compare between single- and multicomponents systems through the introduction of factor (P)



(a)



(b)

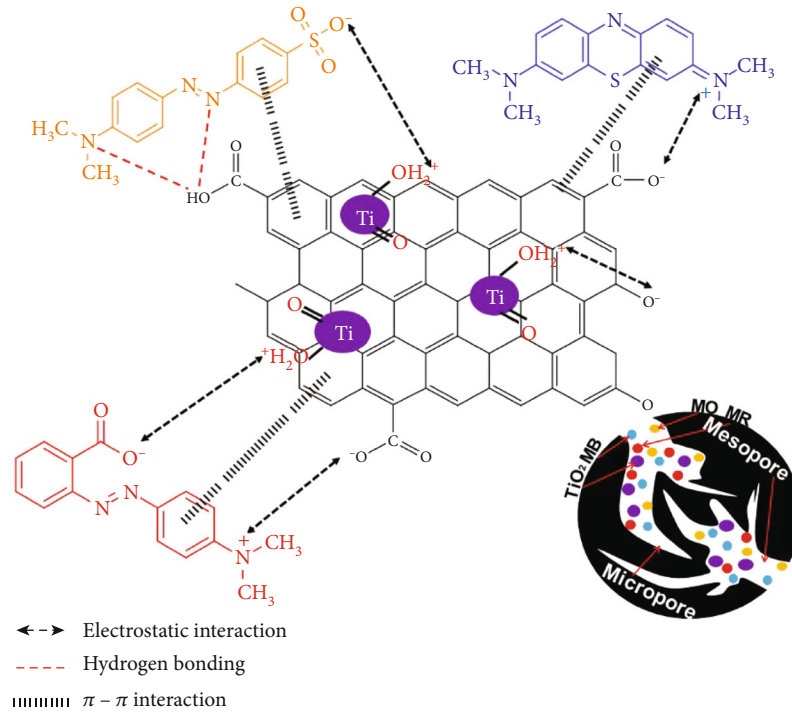
FIGURE 4: (a) pH effect on dye adsorption capacity; (b) The point of zero charge estimated by pH drift method.

(Equation (7)) proposed by McKay and Al Duri [20].

$$P_i = \frac{K_{L,i}/a_{L,i,\text{single}}}{K_{L,i,\text{mul}}/a_{L,i,\text{trinary}}}, \quad (8)$$

where $K_{L,i}/a_{L,i,\text{single}} = q_{L,i,\text{single}}^0$ and $K_{L,i,\text{trinary}}/a_{L,i,\text{trinary}} = q_{L,i,\text{trinary}}^0$ are the maximum monolayer adsorption capacity for component i in a single and trinary systems.

If P -factor < 1 , the adsorption is enhanced by the existence of other components; P -factor = 1, there is no


 SCHEME 2: The diagram of interaction mechanisms of MB, MR, and MO with TiO_2/AC .

noticeable interaction; and P – factor > 1 indicates that the adsorption is suppressed with the existence of other dyes. This model assumes that a Langmuir isotherm for each component (i), the multicomponent isotherm equation can be defined as:

$$q_{e,i,\text{trinary}} = \frac{1}{P_i} \frac{K_{L,i} \cdot C_{e,i,\text{single}}}{1 + a_{L,i} \cdot C_{e,i,\text{trinary}}}, \quad (9)$$

where $a_{L,i}$ is the Langmuir isotherm constants calculated from single solute system.

The IAST is an approach to predict the adsorption isotherms of multiple components solution based on the isotherm data of each individual component considering the thermodynamic consistency of the system. [21]

The Langmuir isotherm in the IAST is developed by using the spreading pressure of component, i , and ψ in integral form proposed by McKay and Al Duri [20].

$$\psi = \frac{\pi \cdot A}{RT} = \int_0^{C_e} \frac{q_e}{C_e} dC_e = \frac{K_L}{a_L} \ln(1 + a_L). \quad (10)$$

Rearranging Equations (3) and (9) [22] to obtain Equations (10) and (11).

$$C_{e,i}^0 = \frac{\exp(\psi(a_{L,i}^0/K_{L,i}^0)) - 1}{a_{L,i}^0}, \quad (11)$$

$$q_{e,i}^0 = \frac{K_{L,i}^0}{a_{L,i}^0} \left[1 - \exp\left(-\psi \left(\frac{a_{L,i}^0}{K_{L,i}^0}\right)\right) \right]. \quad (12)$$

Equation (11) describes the Langmuir isotherm in the IAST at the specified spreading pressure.

The Freundlich isotherm in the IAST is performed by using the spreading pressure in the form of the integral proposed by Kidnay and Myers [23] as in Equation (12).

$$\psi = \frac{\pi \cdot A}{RT} = \int_0^{C_e} \frac{d \ln C_e(q_e)}{d \ln q_e} dq_e = \frac{q_e}{b_F}, \quad (13)$$

$$q_{e,j}^0 = \psi \cdot b_{F,j} \frac{K_{L,i}^0}{a_{L,i}^0}. \quad (14)$$

The Freundlich isotherm in the IAST is as follows:

$$C_{e,j}^0 = \left(\frac{q_{e,j}^0}{a_{F,j}} \right)^{1/b_{F,j}}. \quad (15)$$

By applying the Sips isotherm, the spreading pressure, ψ , can be expressed by [22].

$$\psi = \frac{\pi \cdot A}{RT} = \int_0^{C_e} \frac{q_e}{C_e} dC_e = \frac{q_e}{b_F} \ln(1 + a_S \cdot C_e^{b_S}), \quad (16)$$

$$C_{e,j} = \left(\frac{\exp(\psi(a_{S,i}^0 b_{S,i}^0)/K_{S,i}^0) - 1}{a_{S,i}^0} \right)^{1/b_{S,i}}. \quad (17)$$

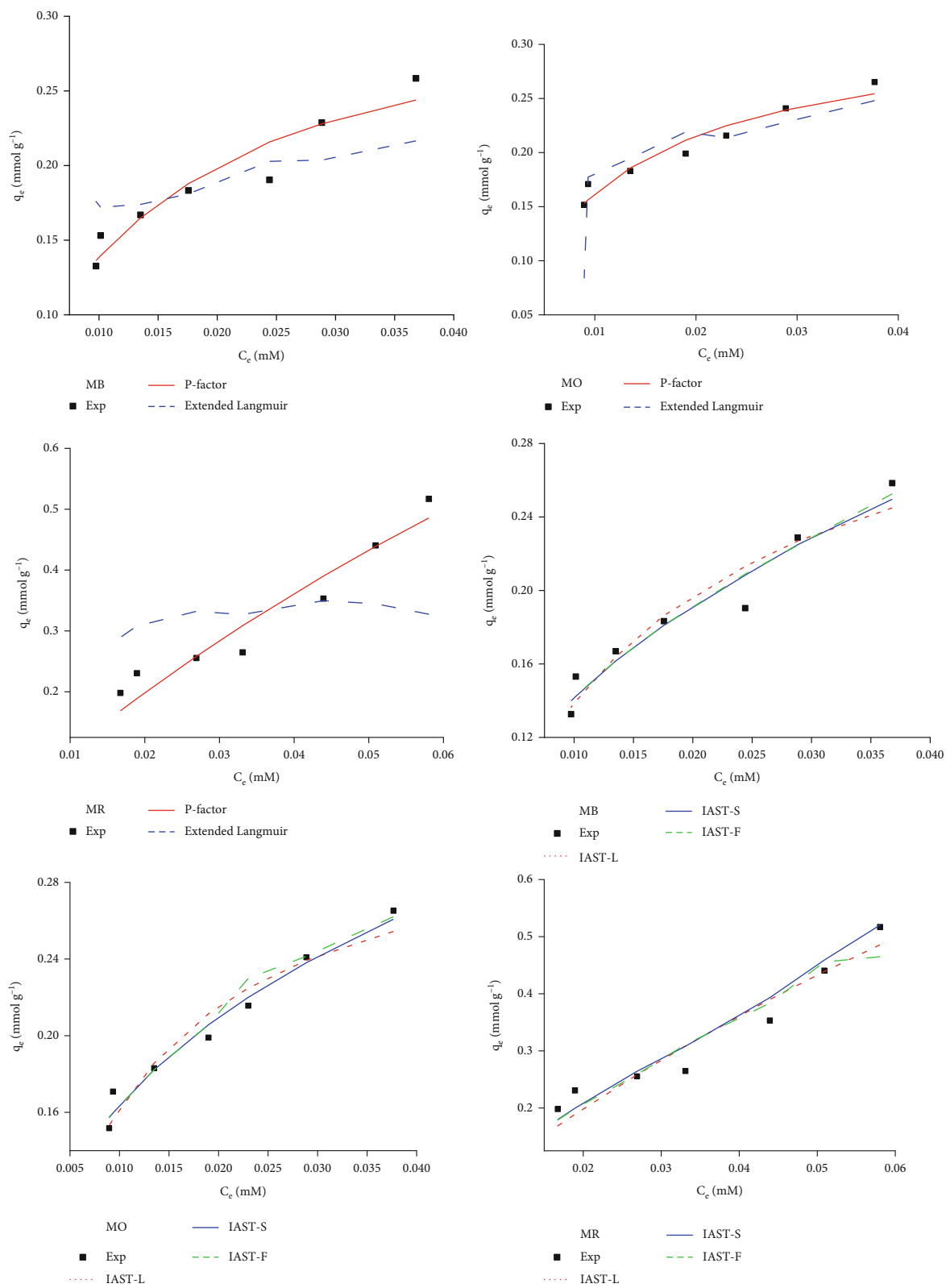


FIGURE 5: The plot of adsorption isotherms for different models.

TABLE 3: The parameters of EL, P-factor, and IAST-sorption isotherm (Langmuir, Freundlich, and Sips), R^2 , and AIC_c values.

Dye	Extended-Langmuir model									R^2	AICs
	$q_{L,MB}^0$ (mmol g ⁻¹)	$q_{L,MO}^0$ (mmol g ⁻¹)	$q_{L,MR}^0$ (mmol g ⁻¹)	$K_{L,MB}^0$ (L.g ⁻¹)	$K_{L,MO}^0$ (L.g ⁻¹)	$K_{L,MR}^0$ (L.g ⁻¹)	$a_{L,MB}^0$ (L.mM ⁻¹)	$a_{L,MO}^0$ (L.mM ⁻¹)	$a_{L,MR}^0$ (L.mM ⁻¹)		
MB	2.274			68.82			30.263			0.576	-48.16
MO		0.60			77.03			127.95		0.900	-37.04
MR			0.80			65.98			82.08	0.674	-29.50
P-factor-Langmuir model											
Dye	$q_{L,MB}^0$ (mmol g ⁻¹)	$q_{L,MO}^0$ (mmol g ⁻¹)	$q_{L,MR}^0$ (mmol g ⁻¹)	$K_{L,MB}^0$ (L.g ⁻¹)	$K_{L,MO}^0$ (L.g ⁻¹)	$K_{L,MR}^0$ (L.g ⁻¹)	$a_{L,MB}^0$ (L.mM ⁻¹)	$a_{L,MO}^0$ (L.mM ⁻¹)	$a_{L,MR}^0$ (L.mM ⁻¹)	R^2	AICs
MB	0.394			26.65			67.63			0.916	-54.34
MO		0.324			33.10			101.9		0.996	-57.86
MR			1.281			6.90			5.40	0.918	-40.47
IAST-Langmuir model											
Dye	$q_{L,MB}^0$ (mmol g ⁻¹)	$q_{L,MO}^0$ (mmol g ⁻¹)	$q_{L,MR}^0$ (mmol g ⁻¹)	$K_{L,MB}^0$ (L.g ⁻¹)	$K_{L,MO}^0$ (L.g ⁻¹)	$K_{L,MR}^0$ (L.g ⁻¹)	$a_{L,MB}^0$ (L.mM ⁻¹)	$a_{L,MO}^0$ (L.mM ⁻¹)	$a_{L,MR}^0$ (L.mM ⁻¹)	R^2	AICs
MB	0.340			23.22			67.63			0.917	-55.34
MO		0.321			32.67			101.86		0.998	-58.86
MR			2.04			10.99			5.40	0.919	-41.47
IAST-Freundlich model											
Dye	$a_{F,MB}$	$a_{F,MO}$	$a_{F,MR}$	$b_{F,MB}$	$b_{F,MO}$	$b_{F,MR}$				R^2	AICs
MB	1.05			0.43						0.996	-58.37
MO		0.843			0.35					0.998	-61.23
MR			6.40			0.89				0.987	-40.92
IAST-Sips model											
Dye	$K_{S,MB}^0$	$K_{S,MO}^0$	$K_{S,MR}^0$	$a_{S,MB}^0$	$a_{S,MO}^0$	$a_{S,MR}^0$	$b_{S,MB}^0$	$b_{S,MO}^0$	$b_{S,MR}^0$	R^2	AICs
MB	1.27			0.44			0.466			0.943	-50.99
MO		1.11			0.60			0.40		0.999	-57.76
MR			16.65			17.5			0.95	0.945	-37.24

The Sips isotherm in the IAST is as follows:

$$q_{e,i}^0 = \frac{K_{S,i}^0}{a_{S,i}^0} \left[1 - \exp \left(\frac{-\psi a_{S,i}^0 b_{S,i}^0}{K_{S,i}^0 - 1} \right) \right]. \quad (18)$$

The model's parameters are by the least square method by minimizing the sum of squared deviations, SSE_S , by means of the numerical optimization techniques using the Solver function in Microsoft Excel. The function for minimization is

$$SSE_S = \sum_1^N \left(y_{\text{exp}} - y_{\text{est}} \right)^2, \quad (19)$$

where y_{exp} is the experimental response, and y_{est} is the response calculated from the model.

The determination coefficient R^2 is obtained according to the expression

$$R^2 = \frac{1 - SSE_S}{SSE_T}, \quad (20)$$

where SSE_T is the total sum of squares equal to $(\sum_1^N (y_{\text{exp}} - y_{\text{mean}}))^2$ (where y_{mean} is the mean value of y).

The AIC (Akaike's information criteria) is used to compare two models. AIC is calculated for each model from Equation (20) [24].

$$AIC = N \cdot \ln \left(\frac{SSE_T}{N} \right) + 2 \cdot N_p + \frac{2 \cdot N_p \cdot (N_p + 1)}{N - N_p - 1}, \quad (21)$$

where N is the number of data points; N_p is the number of parameters fit by the regression.

AIC decides how well the data fit each model. The value of AIC can be positive or negative. The model with the lowest AIC_c score is considered the most likely correct [25].

2.3.3. Recycling of Adsorbent. The recyclability of TiO_2/AC was performed by photocatalytic self-cleaning. After adsorption experiments in 200 mL solution of each dyes at a concentration of 0.0469 mM for MB, 0.0458 mM for MO, and 0.0743 mM for MR in the presence of 0.2 g adsorbent, the used adsorbent, obtained from centrifugation, was desorbed by magnetic stirring under halogen lamp illumination for 2

TABLE 4: A comparison of maximum adsorption capacity based on Langmuir isotherm model of TiO₂/AC with those of other adsorbents reported.

Adsorbents	Adsorption capacity for MB (mmol g ⁻¹)	Adsorption capacity for MO (mmol g ⁻¹)	Adsorption capacity for MR (mmol g ⁻¹)	References
Walnut shell-derived activated carbon	0.251			[37]
Kaolinite	0.062			[38]
Wasted biomass-derived activated carbon	0.048			[34]
Pistachio shell-derived activated carbon	0.430			[39]
TiO ₂ /rice husk-derived activated carbon*	0.452/0.340			The present work
Multiwalled carbon nanotubes		0.157		[40]
Diaminoethane sporopollenin biopolymer		0.014		[41]
Hypercrosslinked polymeric adsorbent		0.217		[42]
Calcined-layered double hydroxides		0.611		[43]
TiO ₂ /rice husk-derived activated carbon*		0.329/0.321		The present work
Apple fruit shell-derived activated carbon			1.615	[44]
Ag@Fe nanoparticles			0.646	[45]
MIL-53(Fe)			0.680	[46]
TiO ₂ /rice husk-derived activated carbon*			0.806/2.04	The present work

*adsorption capacity in single system/trinary system.

hours. The adsorbent was then washed with distilled water and dried at 100°C for further use.

3. Results and Discussion

3.1. Characterization of Materials. Crystal structures of the obtained materials were studied by XRD patterns (Figure 1(a)). XRD patterns of AC exhibit the peaks at 2 theta angles of 29.45, 36.49, 39.49, 43.03, and 47.56° corresponding to (203), (213), (205), (304), and (305) Miller indexes of carbon (JCPDS-00-022-1069). XRD patterns of TiO₂ and composite TiO₂/AC show the characteristic peaks of anatase at 25.25, 38.15, 47.85, 54.65, and 62.75° corresponding to the diffraction plane of (101), (004), (200), (105), and (204) (JCPDS -21-1272). With increasing amount of TiO₂, the intensity of diffraction peaks of anatase increases indicating that two phases of activated carbon and anatase are coexisted. The composition of titanium and carbon elements estimated by EDX is presented in Figure S1. It is found that TiO₂/carbon atomic ratio in product increases with the increase of TiO₂ in initial mixture, indicating that the composition of TiO₂/AC could be controlled by adjusting the reaction composition. Figure 1(b) and Table 1 presents the nitrogen adsorption and desorption isotherms of AC, TiO₂, and TiO₂/AC composites. All the isotherms exhibit a hysteresis loop

which is characteristic for type IV isotherm, confirming the existence of mesoporous materials. The hysteresis loop occurs at relatively high pressures illustrating that the mesoporous structure formed between the particles. The surface area calculated based on the BET model is 1713 m².g⁻¹ for AC, 124 m².g⁻¹ for TiO₂, and 436 m².g⁻¹ for TiO₂/AC. The surface areas of TiO₂ and AC are relatively large compared with previously reported studies [26, 27] showing that the structure of TiO₂ in this study is highly porous. Furthermore, the combination of TiO₂ on AC matrix significantly increased the surface area of TiO₂ itself.

Figures 1(c) and 1(d) show the UV-Vis-DRS and their Tauc's plot for calculating band gap energy derived from UV-Vis-DRS. No energy absorption edge of AC which can be considered as a conductor was observed. The band gap energy of TiO₂ is 3.2 eV which is equivalent to previous report in the range of 3.1-3.2 eV [28]. The combination of TiO₂ with AC gives rise to a red shift in the energy adsorption spectrum, corresponding a band gap energy of 1.9 -2.5 eV illustrating that these composites might have photocatalytic activity in the visible region.

The morphology of TiO₂ prepared from peroxo-hydroxo titanium (IV) complexes consists of fine particles of around 10 nm which can be seen to agglomerate to form larger particles, while AC exhibits the typical layered-structure. In the composite structure, TiO₂ agglomerates are highly dispersed

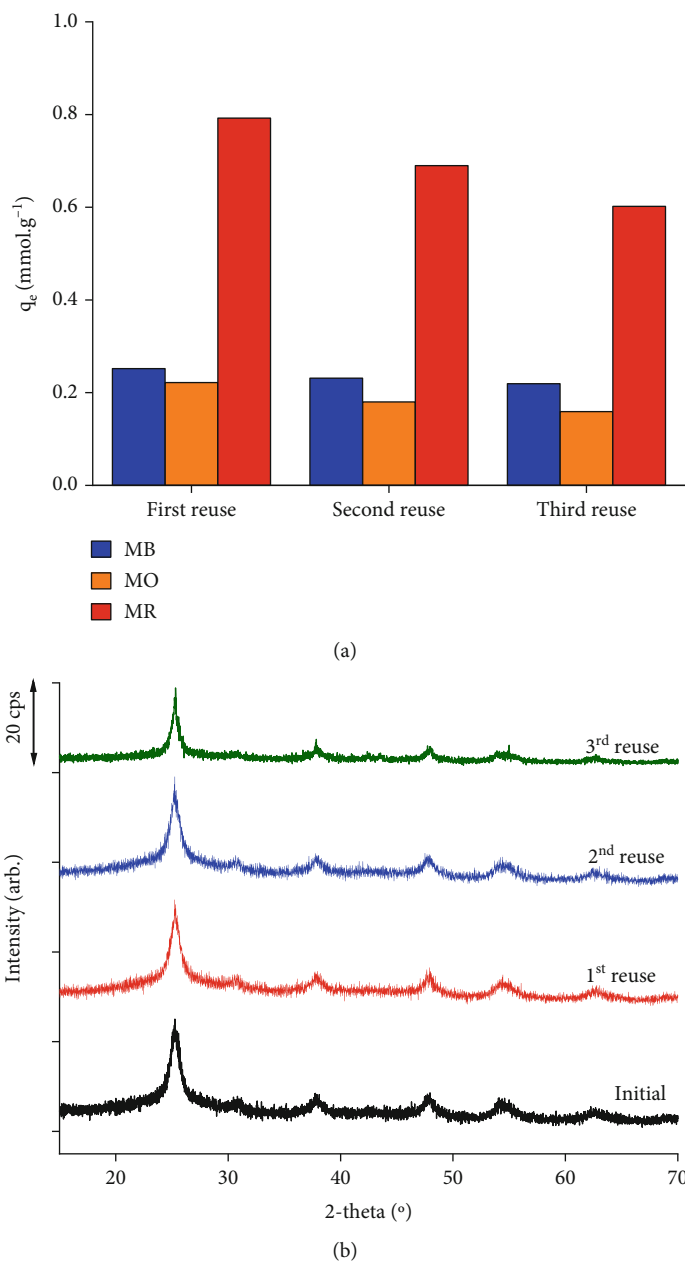


FIGURE 6: (a) Variation of adsorption capacity and (b) XRD patterns of TiO₂/AC and reused TiO₂/AC.

on the AC matrix. The higher TiO₂ content leads to a better coverage of TiO₂ on AC matrix. The distribution of TiO₂ on AC was also studied by EDX mapping. Figure 2 illustrates the elementary mapping of TiO₂/AC (0.5/1) sample. The extensive dispersion of Ti, C, and O elements confirms that TiO₂ was well-distributed on the surface of AC. EDX spectrum also shows some impurity of Mg, Si, Na, and Ca element (of around 0.2-1% w) which might present in rice husks.

3.2. Adsorption Studies

3.2.1. Simultaneous Determination of MB, MO, and MR by UV-Vis Spectroscopy. The dye concentration in solution

was determined by UV-Vis spectroscopy at maximum wavelength of 664 nm for MB, 464 nm for MO, and 500 nm for MR. However, the spectra of three dyes are overlapped resulting in larger error for simultaneous determination of these dyes (Figure 3(a)). In the work, the peaks were deconvoluted by means of OriginPro19/Deconvolution Software as illustrated in Figure 3(b). The deconvoluted UV-Vis spectrum was used to estimate the linear calibration range for dye determination. The linear range of each dye was found to be 0.0063-0.094 mM for MB, 0.015-0.138 mM for MO, and 0.019-0.167 mM for MR. The limit of detections (LODs) for MB, MO, and MR are 0.0007 mM, 0.002 mM, and 0.009 mM, respectively, which are suitable for the detection of these dyes in the adsorption study. Standard addition

method is used to determine the dye in the trinary mixture. The recovery was found to be in the range of 0.9–0.99 indicating that the proposed method could be used for simultaneous determination of MB, MO, and MR (Table S1).

3.2.2. Adsorption Studies of Single Component System of MB, MO, and MR over TiO₂, AC, and TiO₂/AC. The adsorption kinetics of TiO₂, AC, and TiO₂/AC composites at different concentrations of dyes (0.0306–0.0743 mM) are performed in Figure S2 and Table S2. All of samples exhibit the high adsorption towards MB, MO, and MR except only TiO₂ which can adsorb MB. As can be seen from the figure, the higher the dye concentration, the greater the adsorption capacity. This can explain by the fact that the high dye concentration enhances the driving force that overcomes all the mass transfer resistance of dye between the aqueous solution and the surface of adsorbent. The adsorption of dyes is fast in the earlier stage (0–100 minutes) and gradually reached the equilibrium. It is found that the time required to obtain the adsorption/desorption equilibrium was around 120 minutes for all of cases. The kinetics data were applied to the pseudo-first-order and pseudo-second-order kinetic models. The kinetic parameters of the models and R^2 are presented in Table S2. The regression equation based one pseudo-first-order model provides the high values of determination coefficient ($R^2 = 0.88 - 0.98$) and the equilibrium adsorption capacity calculated by this model ($q_{e,cal}$) agrees with equilibrium adsorption capacity obtained by the experiment ($q_{e,exp}$). Hence, the experimental results fit the pseudo-first-order model.

In order to select the TiO₂/AC composite for further study, the removal of MB using TiO₂/AC as a dye model was conducted (Figure S3). The AC exhibits the highest adsorption capacity for MB; whereas, TiO₂ presents a very poor adsorption capacity. The adsorption capacity and the regeneration of spent adsorbent by the photocatalytic self-cleaning are significantly dependent on the composition of TiO₂ in AC. The adsorption capacity was found to be 0.865 mmol g⁻¹ for AC, 0.211 mmol g⁻¹ for TiO₂/AC (0.25/1), 0.452 mmol g⁻¹ for TiO₂/AC (0.5/1), 0.301 mmol g⁻¹ for TiO₂/AC (1/1), 0.251 mmol g⁻¹ for TiO₂/AC (1.5/1), and only 0.2 mmol g⁻¹ for TiO₂. However, after the first recycle, the adsorption capacity of TiO₂/AC(0.5/1) was the highest. Based on the balance between adsorption capacity and visible-light derived photocatalytic self-cleaning, TiO₂/AC (0.5/1) catalyst was selected for further experiments. Figure S4 and Figure S5 present the relationship of equilibrium concentration and adsorption capacity of AC, TiO₂/AC, and TiO₂. Either Langmuir, Freundlich, or Tempkin models describe well the equilibrium data with high determination coefficients ($R^2 = 0.823 - 0.999$) (Table 2) indicating the monolayer adsorption with different energy. The differences between the adsorption capacities of the three dyes may results from different adsorption mechanisms, which might depend on the molecular size and their electron affinities toward adsorbent surface.

3.2.3. Adsorption Isotherms of Trinary Component System for MB, MO, and MR over TiO₂/AC (0.5/1)

(1) *Effect of pH on the Adsorption of TiO₂/AC (0.5/1).* The pH effect on the adsorption of trinary component mixture by TiO₂/AC is presented in Figure 4(a). The MB uptake was found to increase from 0.188 to 0.889 mmol g⁻¹ for an increase in pH from 2 to 5. At higher pH values (5–11), the MB uptake remains almost constant. The point of zero charge of TiO₂/AC obtained by the pH drift method was found at pH = 6.4 (Figure 4(b)). At higher pH (>6.4), the surface of TiO₂/AC may become negatively charged, which promoted the adsorption of the positively charged MB cations (pKa of MB = 3.8 [29]) through electrostatic attraction. This, however, cannot explain its constant adsorption by TiO₂/AC at all the studied pH values. There might be another mode of adsorption, e.g., ion exchange which is similar to the adsorption of MB onto wheat shells [30] or malachite green onto treated sawdust [31].

In contrast, the uptake of MO and MR decreases with the rise of pH. When pH increases from 2 to around 6, the adsorption capacity decreases from 0.344 to 0.124 mmol g⁻¹ for MO and from 0.582 mmol g⁻¹ to 0.452 mmol g⁻¹ for MR. The MO or MR uptake keep unchanged with further pH increasing. Higher adsorptions at lower pH values could be due to protonation properties of the TiO₂/AC. At pH below the point of zero charge (pHs < 6.4), the positive charges at the surface of TiO₂/AC favoured the adsorption of anionic MO and MR (pKa of MO = 3.8 [32] and pKa of MR = 5.1 [33]). A similar trend of adsorption behavior has also been reported with some different adsorbents [34].

In general, the mechanism of dye adsorption is related to the interaction between the adsorbent and the adsorbate in solution. This interaction can occur in many different ways such as hydrogen bonding, electrostatic interaction, π - π stacking interaction, ion-exchange, hydrophobic bonding, and pores and chemical bonding [16, 25, 37, 62, 63] as illustrated in the Scheme 2.

3.2.4. Equilibrium Studies. The equilibrium data of trinary component system were fitted to the extended Langmuir model (EL), the Langmuir model using P-factor models (P-Langmuir model) and Langmuir, Freundlich, and Sips models using IAST (denoted L-IAST, F-IAST, and S-IAST, respectively) as shown in Figure 5. As can be seen, except EL model, the other four models are able to adequately correlate the equilibrium data. Although, the determination coefficient (R^2) is widely used to estimate the goodness of fit for the models with an equal number of experimental points and of the fitting parameters, Akaike information criterion (AIC) is preferred for comparing the models with different parameters. The smaller AICs are, the better the model fit the data. As can be seen from Table 3, it is little difficult to estimate how the AICs are small because there are three values of AICs for each model. Relatively, it can be seen from Table 3 that the AICs are possibly rearranged from low to high based on the sum of AICs as follows: -160.92 (-58.37, -61.23, and -40.92) for F-IAST; -155.67 (-55.34, -58.86, and -41.47) for L-IAST; -152.67 (-54.34, -57.86, and -40.47) for P-factor-Langmuir model; -145.99 (-50.99, -57.76, and -37.24) for S-IAST; and -39.1(-22.96,

-11.83, and -4.31) for EL suggesting both F-IAST model were the best to fit experimental data of all three chosen dyes followed by L-IAST. The Langmuir maximum sorption capacities based on L-IAST model in trinary dyes system were found to be lower than those obtained from the single-dye system, due to the presence of competing dyes. The influence of competitive dyes on the sorption of specific dyes onto the TiO₂/AC is analyzed by using P-factor. The ratios of $q_{L,MR}^0/q_{L,MB}^0$ and $q_{L,MR}^0/q_{L,MO}^0$ are >1, indicating the predominant MR adsorption over MB and MO in both single and trinary systems. The P-values of $Q_{L,MR,single}^0/Q_{L,MR,trinary}^0 = 0.806/2.04 < 1$ prove that the sorption process of MR was promoted by the existence of other dyes, while that of $q_{L,MB,single}^0/q_{L,MB,trinary}^0 = 0.450/0.340 > 1$ presents that the MB adsorption was hindered by the existence of competing dyes. The ratio of $q_{L,MO,single}^0/q_{L,MO,trinary}^0 = 0.329/0.321 \approx 1$ reveals that the MO adsorption is independent on the existence of other dyes. The presence of MB and MO seems to enhance significantly the adsorption capacity of TiO₂/AC toward MR to ~ 2.5 times. MB contains a positively charged amine group while MR and MO contain negatively charged carboxyl and sulfite groups, respectively. It is possible that the MB molecules adsorbed on TiO₂/AC promote the MR adsorption via electrostatic interaction and π - π stacking interaction. The mechanism of complete adsorption of the components is not clear and need to study further.

Table 3 reveals that TiO₂/AC can adsorb as much as approximately two third its own weight (total 763.77 mg (MB + MO + MR)/1000 mg) at ambient temperature. The adsorption capacity of TiO₂/AC was compared with the reported materials for the dye adsorption. The adsorption of MB, MO, or MR in the literature is mostly in single component system (Table 4). One can see that the reported adsorbents include carbon nanotubes, activated carbon, and biopolymers as well as one metal organic framework. However, most of these materials only exhibited lower adsorption capacities than the TiO₂/AC adsorbent or even the MOF, MIL-53(Fe), just possessed an adsorption capacity of 0.668 mM.g⁻¹. Meanwhile, the adsorption capacity in single system/trinary system of TiO₂/AC is 0.452/0.340 for MB, 0.329/0.321 for MO, and 0.806/2.04 for MR. This indicates that the potential using TiO₂/AC to remove dyes is indeed promising.

3.2.5. Recyclability of Adsorbent. The regeneration and reuse of the adsorbent are one of critical criteria for its application in practice. Conventional recycle process is progressed by resining the used adsorbents with organic solvents (ethanol, benzene, and methanol) [35] and heating in limited oxygen environment [36] to elute dyes, resulting in the secondary pollutants and extra cost. Since TiO₂/AC could act as a photocatalytic material, the used TiO₂/AC could be regenerated by self-cleaning when exposed to visible light. Figure 6(a) shows the change in the adsorption capacity of TiO₂/AC after three regenerations by photocatalytic self-cleaning. It can be seen that after the first-cycle regeneration, TiO₂/AC still possessed a comparable adsorption capacity, suggesting

that the photocatalytic self-cleaning was a feasible and effective technique to remove dyes from the used TiO₂/AC. After three reused cycles, TiO₂/AC could still exhibit 96% of its initial adsorption capacity. Figure 6(b) presents the XRD patterns of the reused TiO₂/AC. It was found that there is a slight decrease in intensity but the characteristic peaks of anatase phase still remain unchanged after the recycle process indicating that TiO₂/AC is stable for three recycles.

4. Conclusions

TiO₂/AC materials were synthesized from water soluble titanium hydroperoxide complex and activated carbon from rice husks. The obtained material has high surface area and excellent adsorption capacity to methylene blue, methyl orange, and methyl red compared to the other materials reported. The Freundlich model and Langmuir model in the ideal adsorbed solution theory provide the best prediction to the trinary mixture data in comparison to the extended Langmuir model; Langmuir model using P-factor and Sips model in ideal-adsorbed solution theory. The TiO₂/AC exhibits the excellent reusability by visible light-driven photocatalytic self-cleaning, and their adsorption efficiency was maintained even after three cycles; the change in structure and adsorption capacity of TiO₂/AC was insignificant, proving that this material is durable and has potential for practical applications.

Data Availability

The data used to support the findings of this study are available from the corresponding authors upon request.

Conflicts of Interest

The authors declare that they have no conflicts of interest.

Acknowledgments

This research was financially supported by the Van Lang University, Vietnam, and partially supported by the Hue University under the Core Research Program No. NCM.DHH.2019.08.

Supplementary Materials

Table 1: the recovery in the range of 0.9-0.99 is acceptable indicating that the proposed method could be used for simultaneous determination of MB, MO, and MR. Figure S1: TiO₂/carbon atomic ratio in product analyzed by EDX increases with the increase of TiO₂ in initial mixture, suggesting that the composition of TiO₂/AC could be controlled by adjusting the reaction composition. Figure S2 and Table S2: all of samples present the high adsorption towards MB, MO, and MR expect only TiO₂, which can adsorb MB. The adsorption of dyes is fast in the earlier stage (0-100 minutes) and gradually reached the equilibrium. The experimental data fit the pseudo-first-order model. Figure S3: based on the balance between adsorption capacity and visible-light derived photocatalytic self-cleaning, TiO₂/AC (0.5/1)

catalyst was selected for next experiments. Figure S4: relationship of equilibrium concentration and adsorption capacity of AC, TiO₂/AC, and TiO₂ using Langmuir, Freundlich, or Tempkin models. Figure S5: adsorption isotherms of single component system for MB, MO, and MR over TiO₂/AC (0.5/1). (*Supplementary Materials*)

References

- [1] M. A. Khan, M. I. Khan, and S. Zafar, "Removal of different anionic dyes from aqueous solution by anion exchange membrane," *Membrane Water Treatment*, vol. 8, no. 3, pp. 259–277, 2017.
- [2] V. Vatanpour, H. Karimi, S. Imanian Ghazanlou et al., "Anti-fouling polyethersulfone nanofiltration membranes aided by amine-functionalized boron nitride nanosheets with improved separation performance," *Journal of Environmental Chemical Engineering*, vol. 8, no. 6, article 104454, 2020.
- [3] L. Bulgariu, L. B. Escudero, O. S. Bello et al., "The utilization of leaf-based adsorbents for dyes removal: a review," *Journal of Molecular Liquids*, vol. 276, pp. 728–747, 2019.
- [4] A. George, D. Magimai Antoni Raj, X. Venci et al., "Photocatalytic effect of CuO nanoparticles flower-like 3D nanostructures under visible light irradiation with the degradation of methylene blue (MB) dye for environmental application," *Environmental Research*, vol. 203, article 111880, 2022.
- [5] D. Bhatia, N. R. Sharma, J. Singh, and R. S. Kanwar, "Biological methods for textile dye removal from wastewater: a review," *Critical Reviews in Environmental Science and Technology*, vol. 47, no. 19, pp. 1836–1876, 2017.
- [6] S. Ragupathy, V. Manikandan, S. Devanesan, M. Ahmed, M. Ramamoorthy, and A. Priyadharsan, "Enhanced sun light driven photocatalytic activity of Co doped SnO₂ loaded corn cob activated carbon for methylene blue dye degradation," *Chemosphere*, vol. 295, article 133848, 2022.
- [7] P. Das, P. Debnath, and A. Debnath, "Enhanced sono-assisted adsorptive uptake of malachite green dye onto magnesium ferrite nanoparticles: Kinetic, isotherm and cost analysis," *Environmental Nanotechnology, Monitoring & Management*, vol. 16, article 100506, 2021.
- [8] P. Das, S. Nisa, A. Debnath, and B. Saha, "Enhanced adsorptive removal of toxic anionic dye by novel magnetic polymeric nanocomposite: optimization of process parameters," *Journal of Dispersion Science and Technology*, vol. 43, no. 6, pp. 880–895, 2022.
- [9] A. Deb, A. Debnath, and B. Saha, "Sono-assisted enhanced adsorption of eriochrome black-T dye onto a novel polymeric nanocomposite: kinetic, isotherm, and response surface methodology optimization," *Journal of Dispersion Science and Technology*, vol. 42, no. 11, pp. 1579–1592, 2021.
- [10] P. Das and A. Debnath, "Reactive orange 12 dye adsorption onto magnetically separable CaFe₂O₄ nanoparticles synthesized by simple chemical route: kinetic, isotherm and neural network modeling," *Water Practice Technology*, vol. 16, no. 4, pp. 1141–1158, 2021.
- [11] A. Deb, A. Debnath, K. L. Bhowmik, S. Rudra Paul, and B. Saha, "Application of polyaniline impregnated mixed phase Fe₂O₃, MnFe₂O₄ and ZrO₂ nanocomposite for rapid abatement of binary dyes from aqua matrix: response surface optimisation," *International Journal of Environmental Analytical Chemistry*, pp. 1–19, 2021.
- [12] W. Tian, J. Lin, H. Zhang et al., "Kinetics and mechanism of synergistic adsorption and persulfate activation by N-doped porous carbon for antibiotics removals in single and binary solutions," *Journal of Hazardous Materials*, vol. 423, article 127083, 2022.
- [13] R. Gurav, S. K. Bhatia, T. R. Choi et al., "Adsorptive removal of synthetic plastic components bisphenol-A and solvent black-3 dye from single and binary solutions using pristine pinecone biochar," *Chemosphere*, vol. 296, article 134034, 2022.
- [14] S. Yadav, A. Yadav, N. Bagotia, A. K. Sharma, and S. Kumar, "Novel composites of pennisetum glaucum with CNT: preparation, characterization and application for the removal of safranin O and methylene blue dyes from single and binary systems," *Biomass Convers Biorefinery*, 2022.
- [15] I. Langmuir, "The adsorption of gases on plane surfaces of glass, mica and platinum," *Journal of the American Chemical Society*, vol. 40, no. 9, pp. 1361–1403, 1918.
- [16] H. Freundlich, "Über die adsorption in lösungen," *Zeitschrift für Physikalische Chemie*, vol. 57U, no. 1, pp. 385–470, 1907.
- [17] R. Sips, "On the structure of a catalyst surface," *The Journal of Chemical Physics*, vol. 16, no. 5, pp. 490–495, 1948.
- [18] M. J. Tempkin and V. Pyzhev, "Kinetics of ammonia synthesis on promoted iron catalyst," 2022, https://www.researchgate.net/publication/306535741_Kinetics_of_ammonia_synthesis_on_promoted_iron_catalyst.
- [19] J. A. V. Butler and C. Ockrent, "Studies in electrocapillarity. III," *The Journal of Physical Chemistry*, vol. 34, no. 12, pp. 2841–2859, 1930.
- [20] G. McKay and B. Al Duri, "Ein vereinfachtes modell für das adsorptionsgleichgewicht von mischungen aus farbstoffen an aktivkohle," *Chemical Engineering and Processing Process Intensification*, vol. 22, no. 3, pp. 145–156, 1987.
- [21] A. Myers and J. Praunitz, "Thermodynamics of photosynthesis," *Biophysics (Oxf)*, vol. 9, no. 3, pp. 316–321, 1964.
- [22] K. K. H. Choy, J. F. Porter, and G. McKay, "Single and multi-component equilibrium studies for the adsorption of acidic dyes on carbon from effluents," *Langmuir*, vol. 20, no. 22, pp. 9646–9656, 2004.
- [23] A. J. Kidnay and A. L. Myers, "A simplified method for the prediction of multicomponent adsorption equilibria from single gas isotherms," *AIChE Journal*, vol. 12, no. 5, pp. 981–986, 1966.
- [24] H. Motulsky and A. Christopoulos, *Fitting Models to Biological Data Using Linear and Nonlinear Regression. Fitting Curves with GraphPad Prism*, GraphPad Prism Softw. Inc, San Diego, California, 2003.
- [25] N. T. Thanh Tu, T. V. Thien, P. D. Du, V. T. Thanh Chau, T. X. Mau, and D. Q. Khieu, "Adsorptive removal of Congo red from aqueous solution using zeolitic imidazolate framework-67," *Journal of Environmental Chemical Engineering*, vol. 6, no. 2, pp. 2269–2280, 2018.
- [26] N. Yalçın and V. Sevinç, "Studies of the surface area and porosity of activated carbons prepared from rice husks," *Carbon N. Y*, vol. 38, no. 14, pp. 1943–1945, 2000.
- [27] S. Xiong, Y. Tang, H. S. Ng et al., "Specific surface area of titanium dioxide (TiO₂) particles influences cyto- and photo-toxicity," *Toxicology*, vol. 304, pp. 132–140, 2013.
- [28] S. K. S. K. S. Saranya, V. Vellora Thekkae Padil, C. Senan et al., "Green synthesis of high temperature stable anatase titanium dioxide nanoparticles using gum kondagogu: characterization

- and solar driven photocatalytic degradation of organic dye,” *Nanomaterials*, vol. 8, no. 12, p. 1002, 2018.
- [29] J. R. Kim and E. Kan, “Heterogeneous photo-Fenton oxidation of methylene blue using CdS-carbon nanotube/TiO₂ under visible light,” *Journal of Industrial and Engineering Chemistry*, vol. 21, pp. 644–652, 2015.
- [30] Y. Bulut and H. Aydin, “A kinetics and thermodynamics study of methylene blue adsorption on wheat shells,” *Desalination*, vol. 194, no. 1–3, pp. 259–267, 2006.
- [31] V. K. Garg, R. Gupta, A. B. Yadav, and R. Kumar, “Dye removal from aqueous solution by adsorption on treated sawdust,” *Bioresource Technology*, vol. 89, no. 2, pp. 121–124, 2003.
- [32] S. G. Richard, H. Gary, W. Robert, and E. Edward, “Kinetics of Acid dissociation ion recombination of aqueous methyl orange,” vol. 2240, no. 26, pp. 2–4, 1989.
- [33] R. K. Srour and L. M. McDonald, “Determination of the acidity constants of methyl red and phenol red indicators in binary methanol– and ethanol-water mixtures,” *Journal of Chemical & Engineering Data*, vol. 53, no. 1, pp. 116–127, 2008.
- [34] N. Mohammadi, H. Khani, V. K. Gupta, E. Amereh, and S. Agarwal, “Adsorption process of methyl orange dye onto mesoporous carbon material- kinetic and thermodynamic studies,” *Journal of Colloid and Interface Science*, vol. 362, no. 2, pp. 457–462, 2011.
- [35] K. Y. A. Lin and H. A. Chang, “Ultra-high adsorption capacity of zeolitic imidazole framework-67 (ZIF-67) for removal of malachite green from water,” *Chemosphere*, vol. 139, pp. 624–631, 2015.
- [36] D. Guo, Y. Li, B. Cui et al., “Natural adsorption of methylene blue by waste fallen leaves of *Magnoliaceae* and its repeated thermal regeneration for reuse,” *Journal of Cleaner Production*, vol. 267, p. 121903, 2020.
- [37] M. Liu, X. Li, Y. Du, and R. Han, “Adsorption of methyl blue from solution using walnut shell and reuse in a secondary adsorption for Congo red,” *Bioresource Technology Reports*, vol. 5, pp. 238–242, 2019.
- [38] D. Ghosh and K. G. Bhattacharyya, “Adsorption of methylene blue on kaolinite,” *Applied Clay Science*, vol. 20, no. 6, pp. 295–300, 2002.
- [39] A. A. Attia, B. S. Girgis, and S. A. Khedr, “Capacity of activated carbon derived from pistachio shells by H₃PO₄ in the removal of dyes and phenolics,” *Journal of Chemical Technology and Biotechnology*, vol. 78, no. 6, pp. 611–619, 2003.
- [40] Y. Yao, H. Bing, X. Feifei, and C. Xiaofeng, “Equilibrium and kinetic studies of methyl orange adsorption on multiwalled carbon nanotubes,” *Chemical Engineering Journal*, vol. 170, no. 1, pp. 82–89, 2011.
- [41] M. Küçükosmanoğlu, O. Gezici, and A. Ayar, “The adsorption behaviors of methylene blue and methyl orange in a diaminoethane sporopollenin-mediated column system,” *Separation and Purification Technology*, vol. 52, no. 2, pp. 280–287, 2006.
- [42] J. H. Huang, K. L. Huang, S. Q. Liu, A. T. Wang, and C. Yan, “Adsorption of Rhodamine B and methyl orange on a hypercrosslinked polymeric adsorbent in aqueous solution,” *Colloids and Surfaces A: Physicochemical and Engineering Aspects*, vol. 330, no. 1, pp. 55–61, 2008.
- [43] Z. M. Ni, S. J. Xia, L. G. Wang, F. F. Xing, and G. X. Pan, “Treatment of methyl orange by calcined layered double hydroxides in aqueous solution: adsorption property and kinetic studies,” *Journal of Colloid and Interface Science*, vol. 316, no. 2, pp. 284–291, 2007.
- [44] E. A. Khan and T. A. K. Shahjahan, “Adsorption of methyl red on activated carbon derived from custard apple *Annona squamosa* fruit shell: equilibrium isotherm and kinetic studies,” *Journal of Molecular Liquids*, vol. 249, pp. 1195–1211, 2018.
- [45] Z. Zaheer, A. AL-Asfar, and E. S. Aazam, “Adsorption of methyl red on biogenic nanocomposite adsorbent: isotherms, kinetics and mechanisms,” *Journal of Molecular Liquids*, vol. 283, pp. 287–298, 2019.
- [46] E. Yilmaz, E. Sert, and F. S. Atalay, “Synthesis, characterization of a metal organic framework: MIL-53 (Fe) and adsorption mechanisms of methyl red onto MIL-53 (Fe),” *Journal of the Taiwan Institute of Chemical Engineers*, vol. 65, pp. 323–330, 2016.